

TRPM7 senses oxidative stress to release Zn²⁺ from unique intracellular vesicles

Sunday A. Abiria^{a,b,c}, Grigory Krapivinsky^{a,b,c}, Rajan Sah^d, Ana G. Santa-Cruz^{a,b,c}, Dipayan Chaudhuri^e, Jin Zhang^{a,b,c}, Pichet Adstamongkonkul^f, Paul G. DeCaen^g, and David E. Clapham^{a,b,c,1}

^aHoward Hughes Medical Institute, Boston Children's Hospital, Boston, MA 02115; ^bDepartment of Cardiology, Boston Children's Hospital, Boston, MA 02115; ^cDepartment of Neurobiology, Harvard Medical School, Boston, MA 02115; ^dDepartment of Internal Medicine, University of Iowa, Iowa City, IA 52242; ^eNora Eccles Harrison Cardiovascular Research and Training Institute, Division of Cardiology, Department of Internal Medicine, University of Utah, Salt Lake City, UT 84112; ^fSchool of Engineering and Applied Sciences, Harvard University, Cambridge, MA 02138; and ^gDepartment of Pharmacology, Northwestern University, Chicago, IL 60611

Contributed by David E. Clapham, June 16, 2017 (sent for review May 3, 2017; reviewed by Michael D. Cahalan, Dejian Ren, and Haoxing Xu)

TRPM7 (transient receptor potential cation channel subfamily M member 7) regulates gene expression and stress-induced cytotoxicity and is required in early embryogenesis through organ development. Here, we show that the majority of TRPM7 is localized in abundant intracellular vesicles. These vesicles (M7Vs) are distinct from endosomes, lysosomes, and other familiar vesicles or organelles. M7Vs accumulate Zn²⁺ in a glutathione-enriched, reduced lumen when cytosolic Zn²⁺ concentrations are elevated. Treatments that increase reactive oxygen species (ROS) trigger TRPM7-dependent Zn²⁺ release from the vesicles, whereas reduced glutathione prevents TRPM7-dependent cytosolic Zn²⁺ influx. These observations strongly support the notion that ROS-mediated TRPM7 activation releases Zn²⁺ from intracellular vesicles after Zn²⁺ overload. Like the endoplasmic reticulum, these vesicles are a distributed system for divalent cation uptake and release, but in this case the primary divalent ion is Zn²⁺ rather than Ca²⁺.

TRPM7 | zinc | vesicles

TRPM7 (transient receptor potential cation channel subfamily M member 7), an ion channel and cytoplasmic kinase, is ubiquitously expressed and essential in early embryonic development (1–4) but also may mediate oxidative stress-induced anoxic neuronal death in adults (5, 6). As an ion channel, TRPM7 conducts Zn²⁺ > Mg²⁺ ~ Ca²⁺ and monovalent cations (7–10) and contributes to labile cytosolic and nuclear Zn²⁺ concentrations (8). TRPM7's C-terminal kinase can phosphorylate multiple substrates (11–13) and is cleaved to release a proapoptotic, chromatin-modifying enzyme (8, 14). Zn²⁺ regulates TRPM7's kinase activity (11) and binding to transcription factors (8). It is a potent signal for many cellular processes previously related to TRPM7 function, including gene expression, mitosis, and cell survival, but is also proapoptotic at extreme concentrations (15–18).

TRPM7 has been proposed to regulate intracellular Mg²⁺ levels (19). However, as we have shown, *Trpm7*^{-/-} cells have normal total magnesium concentrations (3, 14), with the many abundant magnesium transporters (20) probably accounting for normal Mg²⁺ homeostasis. Under physiological conditions, plasma membrane TRPM7's inward conductance is miniscule (<10 pA/pF at -100 mV), but it increases over minutes if the free cytosolic Mg²⁺ concentration falls below its normal level of ~0.5–1 mM (21). Because in most cells the primary buffers for Mg²⁺ are phosphonucleotides (22), the metabolic state potentially regulates TRPM7 activity as ATP levels rise and fall around 0.5 mM. Under normal circumstances, the driving force for Mg²⁺ entry into cells is relatively low ($[Mg^{2+}]_o = 1$ mM vs. $[Mg^{2+}]_i \sim 1$ mM; $E_{Mg} = 0$ mV) compared with Ca²⁺ ($[Ca^{2+}]_o = 2$ mM vs. $[Ca^{2+}]_i \sim 100$ nM; $E_{Ca} = +125$ mV) or Zn²⁺ ($[Zn^{2+}]_o = 1$ –300 μM vs. $[Zn^{2+}]_i \sim 0.5$ nM; $E_{Zn} = +100$ mV, with 1 μM $[Zn^{2+}]_o$). Few Zn²⁺-permeant channels are known, however, and the many putative Zn²⁺ transporters (>20 ZnT/SLC30 and ZIP/SLC39 in humans) primarily regulate $[Zn^{2+}]$ in organelles and the cytosol

(23). TRPM7's Zn²⁺ conductance suggests that it could support rapid changes in cytoplasmic Zn²⁺ levels under the right circumstances, either across the plasma membrane or from intracellular compartments.

Oxidative stress increases inward divalent ion permeation through TRPM7 (5, 9), whereas acute and chronic oxidative stress in culture (24–26) or during ischemia–reperfusion in vivo (27, 28) induces TRPM7 expression. The resulting increase in cytosolic Zn²⁺ could result in toxic cytosolic concentrations (9). Conversely, reduction of TRPM7 expression protects animals from postischemia reperfusion (5), a condition typically accompanied by increased reactive oxygen species (ROS) and Zn²⁺ release from intracellular stores (29). Physiological redox transitions required for stem cell differentiation and gene expression during embryonic development (30, 31) may also be sensed by TRPM7 and transduced via Zn²⁺-dependent signals (32).

Because TRPM7 patch-clamp recording is limited to the plasma membrane, the assumption has been that TRPM7's main function is on the plasma membrane. However, we have previously shown that TRPM7 is also on intracellular membranes (33–35). Indeed, ROS activation of divalent ion influx through TRPM7 (5, 9) is reminiscent of ROS activation of TRPM2, which releases Ca²⁺ and Zn²⁺ from lysosomes (36, 37). Here we show that TRPM7 is an intracellular Zn²⁺ release channel located on previously

Significance

TRPM7 (transient receptor potential cation channel subfamily M member 7) is required for normal organ development but also mediates anoxic neuronal death. TRPM7 contains a channel that conducts cations into the cytosol and C-terminal kinase that can phosphorylate multiple substrates. The kinase is cleaved to regulate gene expression and apoptosis. The link between TRPM7's channel and its organismal function remains the least understood aspect of TRPM7. Here, we identify intracellular Zn²⁺ storage vesicles that contain the majority of TRPM7 protein. TRPM7 senses reactive oxygen species (ROS) to release Zn²⁺ from these vesicles. Just as the endoplasmic reticulum sequesters and releases Ca²⁺, we propose that these vesicles fulfill a similar function for Zn²⁺ and that TRPM7 coordinates fluctuations in cellular $[Zn^{2+}]$ and ROS during development and injury.

Author contributions: S.A.A., G.K., and D.E.C. designed research; S.A.A., G.K., R.S., A.G.S.-C., D.C., J.Z., P.A., and P.G.D. performed research; R.S. contributed new reagents/analytic tools; S.A.A., G.K., R.S., A.G.S.-C., D.C., P.G.D., and D.E.C. analyzed data; and S.A.A., G.K., A.G.S.-C., D.C., P.G.D., and D.E.C. wrote the paper.

Reviewers: M.D.C., University of California, Irvine; D.R., University of Pennsylvania; and H.X., University of Michigan.

The authors declare no conflict of interest.

¹To whom correspondence should be addressed. Email: dclapham@enders.tch.harvard.edu.

This article contains supporting information online at www.pnas.org/lookup/suppl/doi:10.1073/pnas.1707380114/-DCSupplemental.

uncharacterized vesicles (M7Vs) that are distinct from familiar organelles. These vesicles sequester Zn^{2+} during cytosolic overload. We show that the intravesicular M7V environment is reducing and that oxidation induces TRPM7-dependent Zn^{2+} release from these vesicles. We hypothesize that TRPM7-mediated Zn^{2+} release from intracellular stores regulates ROS signaling events during embryonic development or postnatal stress/injury.

Results

TRPM7 Is Most Abundant on Intracellular Vesicles. Whole-cell patch-clamp measurements of endogenous and ectopically expressed TRPM7 establish that it is present in the plasma membrane (1, 2). As with many ion channels that are relatively sparse, ectopically expressed TRPM7 was undetected at the plasma membrane by immunocytochemistry (Fig. 1A). Instead TRPM7 was detected largely in intracellular vesicles (Fig. 1A–E) in multiple cell types. To rule out TRPM7 mislocalization artifacts caused by ectopic overexpression, we used a gene-trap strategy to insert GFP at the N terminus of endogenous TRPM7 in mouse ES cells. Expression of full-length GFP-TRPM7 was confirmed by immunoprecipitation of TRPM7 using either anti-GFP or anti-TRPM7, followed by Western blotting (Fig. S1A). Endogenous

GFP-TRPM7, visualized by immunostaining with anti-GFP antibody, was abundant in intracellular vesicles similar in size and distribution to TRPM-positive vesicles in cells ectopically expressing TRPM7 (Fig. 1F). We also coimmunostained cells for GFP (TRPM7) and β -actin, which lines the inner leaflet of plasma membrane (38), and imaged the localization of both proteins by stimulated emission depletion (STED) microscopy. β -Actin was concentrated at the cell periphery in a punctate distribution at the plasma membrane, whereas TRPM7 was detected in \sim 100-nm vesicles located only on the cytoplasmic side relative to β -actin (Fig. 1B).

To determine the intracellular localization of TRPM7 in detail, we carried out transmission electron microscopy (TEM) of anti-GFP-labeled HEK293 cells expressing TRPM7 with a pH-sensitive GFP (pHluorin) (39) inserted into the S1/2 loop. Insertion of tags into the S1/2 loop did not compromise TRPM7 channel function (Fig. S2). TEM revealed unilamellar vesicles with an average diameter of \sim 150 nm specifically labeled with anti-GFP (Fig. 1C and Fig. S1B and C). The luminal anti-GFP labeling demonstrates the expected membrane orientation of TRPM7 polypeptide with the S1/2 loop in the lumen and the N and C termini in the cytosol (Fig. 1C). Imaging of live cells

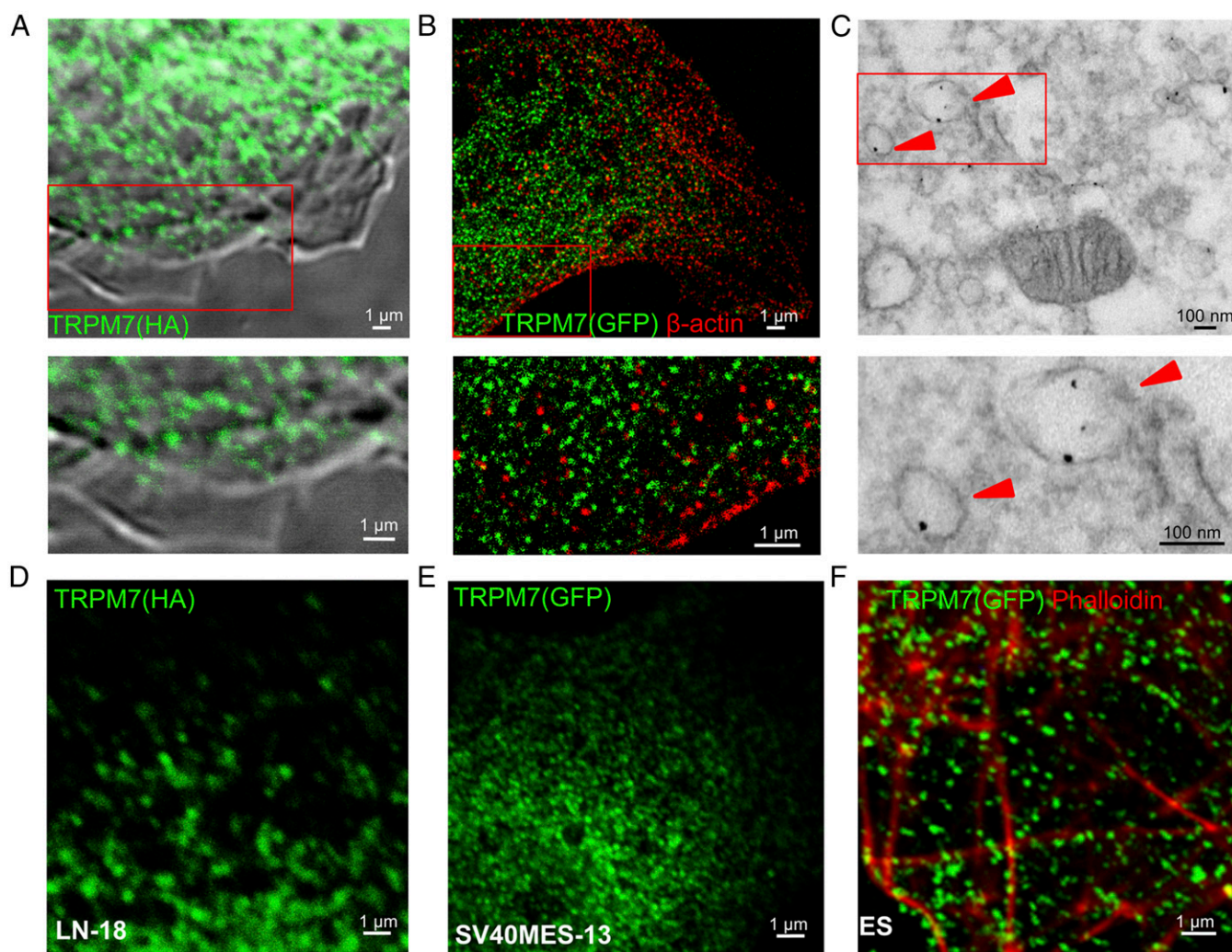


Fig. 1. Vesicular localization of TRPM7. (A) Immunofluorescence and differential interference contrast (DIC) images of an HEK293 cell expressing TRPM7-HA. (B and C) Superresolution (B) and transmission electron micrographs (C) of an HEK293 cell expressing TRPM7 tagged with GFP positioned on intravesicular residues (arrowheads indicate anti-GFP immunogold-labeled vesicles). (D and E) Vesicular localization of TRPM7 stably expressed in LN-18 glioma cells (D) and in SV40MES-13 glomerular mesangial cells (E). (F) Endogenous TRPM7 in mouse ES cells genetically tagged with GFP (see Fig. S1 and Movie S1).

expressing the pHluorin-tagged TRPM7 established that the vesicles are acidic (Fig. S1D). Total internal reflection (TIRF) microscopy of GFP-tagged TRPM7 in live SV40MES-13 cells also revealed TRPM7 localization in vesicles (Movie S1). Thus, under all conditions examined, TRPM7 channels are located primarily on abundant intracellular vesicles with comparatively fewer numbers on the plasma membrane.

M7Vs Are Distinct from Well-Characterized, Membrane-Bound Intracellular Compartments. To determine whether M7Vs are simply in route to the plasma membrane via classical secretory pathways, we assessed the colocalization of TRPM7 and GFP-tagged vesicular stomatitis virus protein (VSVG-GFP) (40). TRPM7 did not colocalize with VSVG-GFP in transport vesicles in the cytoplasm or at the plasma membrane (Fig. 2A). Moreover, the vesicles did not colocalize with markers of several known cellular compartments, including calnexin, DIER, Sec61 β (endoplasmic reticulum; ER), PEX19, RFP-PTS (immature and mature peroxisomes), lamp1 (lysosomes), clathrin (endosomes), edem1 [EDEMosomes, ER-derived ERAD-tuning vesicles (41)], ergic-53 (ER–Golgi intermediate compartments), and tyrosinase (melanosomes) (Fig. 2B). M7Vs are also smaller and more abundant than zincosomes, ~1- μ m-wide vesicles that fluoresce brightly upon cellular Zn²⁺ overload (42). From their morphology, lack of markers, and lack of fusion with the plasma membrane by various stimuli (34), we surmise that M7Vs are previously uncharacterized intracellular membrane compartments.

Purification of M7Vs. Sucrose gradient fractionation confirms that endogenous TRPM7 is predominantly intracellular because it migrates as a peak distinct from the plasma membrane marker Na⁺/K⁺ ATPase (Fig. 3A). To probe the cellular function of TRPM7 vesicles, we isolated TRPM7-containing vesicles from postnuclear supernatants (PNS). We first tagged the C terminus of TRPM7 with an HA epitope and pulled down M7Vs with anti-HA-conjugated magnetic nanoparticles. The pull-down appears specific, because excess HA peptide blocked vesicle binding, the vesicles colocalized with nanoparticles, and the vesicle preparation was depleted of contaminating mitochondrial and endoplasmic reticulum markers (Fig. 3). We performed a second affinity purification of vesicles by N-terminal FLAG tag after elution of anti-HA-bound vesicles for proteomic analysis (Fig. S3A). The affinity binding of the vesicles via tags located on the N and C terminals supports our earlier conclusion that the termini of TRPM7 face the cytoplasm. The substantial reduction of ER and mitochondria (Fig. 3D and Fig. S3A) supports the conclusion that TRPM7 vesicles are distinct from these structures.

The M7V Proteome. TRPM7 was enriched in the vesicle proteome, with a SILAC (stable isotope labeling with amino acids in cell culture) ratio of 56 in HEK293 cells and 98 in SV40MES-13 cells (Dataset S1). Proteins in known cellular compartments such as mitochondria, Golgi, and ER were present in the vesicle proteome, but ~60% of the proteome was not classified in the Panther System (Dataset S1). We then screened the unclassified candidate proteins as potential markers for M7Vs and observed colocalization of M7Vs and vesicular integral membrane protein-36 (VIP36, also known as “LMAN2”) (Fig. S3B). VIP36 is an intracellular lectin of unknown function and has been observed in the ER–Golgi intermediate compartment and post-Golgi vesicles (43–45). VIP36 contains a single transmembrane domain with a luminal N terminus (46) that is ideal for targeting sensors into M7Vs (see below).

Purified M7Vs Accumulate Zn²⁺. TRPM7’s extracellular domains face the lumen of the M7V (Figs. 1C and 3B–D), and thus inward cationic current should flow from the vesicular lumen into the cytoplasm under ionic conditions identical to those at the plasma membrane. Purified M7Vs immobilized on Cell-Tak-coated

coverslips were loaded with the fluorescent divalent indicators Fluo4-AM (K_d , Ca²⁺ = 335 nM), MagFluo4-AM (K_d , Mg²⁺ = 4.7 mM), or FluoZin-3-AM (K_d , Zn²⁺ = 15 nM) (Methods). These vesicles were permeant to Ca²⁺, Mg²⁺, or Zn²⁺ applied in the bath, but only Zn²⁺ remained trapped in the vesicles after extravesicular divalent ions were washed away (Fig. 4A–D and Fig. S4A and B). Accumulated intravesicular Zn²⁺ then was chelated with membrane-permeant TPEN [*N,N,N',N'*-tetrakis(2-pyridylmethyl) ethylenediamine], decreasing indicator fluorescence (Fig. 4C and D). To rule out the possibility that Zn²⁺ was trapped by FluoZin-3, we loaded the vesicles with Zn²⁺ in the absence of FluoZin-3, washed out extravesicular Zn²⁺, and loaded the vesicles with FluoZin-3-AM. FluoZin-3 fluorescence increased to saturation over 10 min and remained at these levels after the extravesicular fluorophore was washed out (Fig. 4E and F). These data show that purified M7Vs are capable of selectively accumulating Zn²⁺.

M7Vs Accumulate Zn²⁺ in Intact Cells. To study vesicular Zn²⁺ in intact cells, we targeted two genetically encoded Zn²⁺ sensors to the M7V lumen. We created an intravesicular Zn²⁺ sensor by targeting eCALWY4 (47) to the TRPM7 vesicle lumen by fusion of VIP36’s N-terminal 36 amino acids (including the signal peptide) to eCALWY4’s N terminus (Fig. 5B). Resistance to proteinase-K digestion indicated that the sensor was inside the vesicle (Fig. 5D). The intravesicular sensor did not respond to membrane-permeant TPEN but was responsive to increased luminal [Zn²⁺] (Fig. 5E), indicating low intravesicular free [Zn²⁺]. The Zn²⁺-binding constant of the vesicular VIP36-eCALWY4 sensor (0.36 ± 06 nM) was determined simultaneously with that of the nuclear Zn²⁺ sensor, ZapCmR2-NLS (48) (0.41 ± 07 nM), as a reference. Both binding constants were comparable to the Zn²⁺-binding constants of eCALWY4 (0.63 nM) (47) and Zap1 (0.81 nM) (49) (Fig. S5A). The calculation of Zn²⁺ concentrations using the binding constant suggests that the vesicles contain <0.1 nM free Zn²⁺ under resting conditions. To rule out any possible effects of vesicular pH on the sensor’s Zn²⁺ affinity, we showed that neutralization of the vesicular lumen with NH₄Cl did not increase FRET (Fig. S5B). In contrast to M7Vs, ER-localized Sec61 β -eCALWY4 (Fig. 5C) was saturated with Zn²⁺ under resting conditions (Fig. 5F), consistent with previously reported storage of Zn²⁺ in the ER (50).

Next, we tested M7V cytosolic Zn²⁺ sequestration. Increasing extracellular [Zn²⁺] increased cytosolic [Zn²⁺] to >4 nM ($\tau = 104 \pm 4$ s) (Fig. 5G; see also ref. 49), followed by slower vesicular uptake ($\tau = 503 \pm 90$ s) (Fig. 5G). Vesicular Zn²⁺ entry continued after influx was stopped by extracellular Zn²⁺ chelation with EGTA (Fig. 5H). We also targeted a recently developed intensometric Zn²⁺ sensor, ZnGreen1 (51), to the M7V lumen by inserting it into the S1/2 intraluminal loop of TRPM7. M7Vs containing ZnGreen1 did not contain TPEN-chelatable Zn²⁺ (Fig. S5C) but took up Zn²⁺ after cytosolic Zn²⁺ elevation (Fig. 5I and Fig. S5D); cytosolic and M7V-luminal ZnGreen1 have similar Zn²⁺ equilibrium binding constants of 2.1–2.9 nM (Fig. S5E and F). ZnGreen1-tagged TRPM7 channels were also functional (Fig. S2A).

To test whether vesicles in intact cells retain loaded Zn²⁺, we took advantage of the low Zn²⁺ affinity and wide dynamic range of ZnGreen1 (Fig. S5E and F), enabling us to monitor changes in Zn²⁺ that otherwise would saturate eCALWY sensors (47). As shown in Fig. S5D–F, elevation of extracellular [Zn²⁺] to 500 μ M elevated cytosolic and M7V [Zn²⁺] to >40 nM, saturating ZnGreen1. When cells were allowed to recover for 15 min in culture medium at 37 °C (Fig. 5J), cytosolic ZnGreen1 fluorescence was no longer saturated, but the vesicular sensor remained saturated (Fig. 5K and L). These results indicate that Zn²⁺ was enriched in M7Vs relative to the cytoplasm.

To examine whether divalent cation retention in M7Vs was selective for Zn²⁺, we also imaged Ca²⁺ uptake and release from

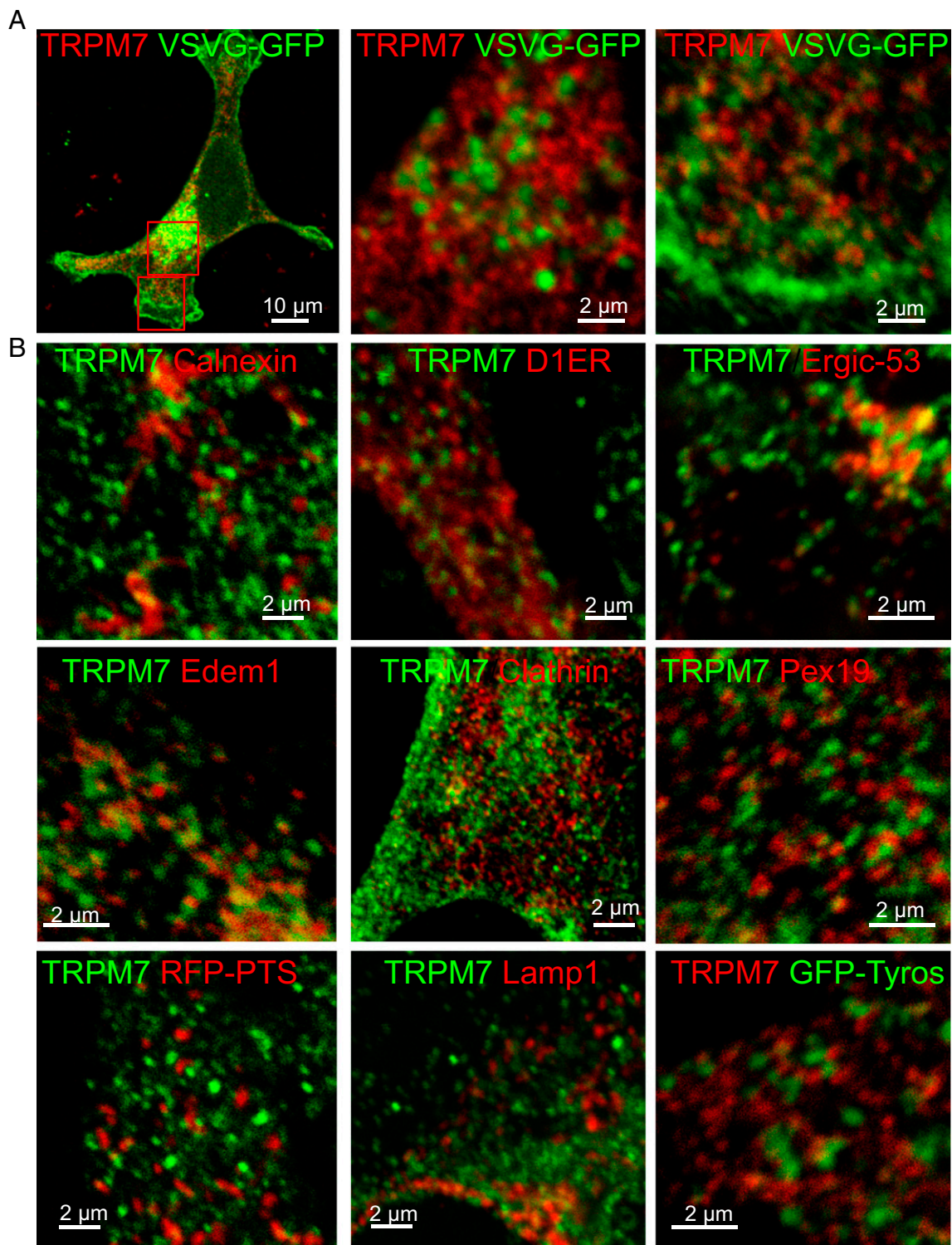


Fig. 2. M7Vs are distinct from well-characterized intracellular vesicular compartments. (A) Immunocytochemistry of VSVG-GFP and TRPM7-HA vesicles in HEK293 cells. (B) Absence of colocalization of TRPM7-HA and markers of the ER (Calnexin), EDEMosomes (Edem1), the tyrosinase ER–Golgi intermediate compartment, peroxisomes (RFP-PTS and Pex19), lysosomes (Lamp1), melanosomes (Tyrosinase or Tyros), or clathrin-coated endosomes. See Table S1 for additional description of markers.

M7Vs in situ using GCaMP6s (52). This probe was also inserted in the S1/2 loop of TRPM7 (Fig. S4 C and D) and did not alter channel function (Fig. S2B). The addition of 100 μM ATP to intact cells triggered Ca^{2+} spikes in M7Vs that were synchronous with ER Ca^{2+} release (simultaneously monitored with the red

fluorescent, ER-targeted Ca^{2+} sensor, RCEPIAer) (Fig. S4C) (53) or cytosolic spikes (simultaneously monitored with cytosolic red fluorescent R-GECO1) (Fig. S4D) (54). The equilibration of Ca^{2+} between the cytosol and M7Vs is consistent with the lack of Ca^{2+} trapping in vesicles in vitro (Fig. S4A) and supports our

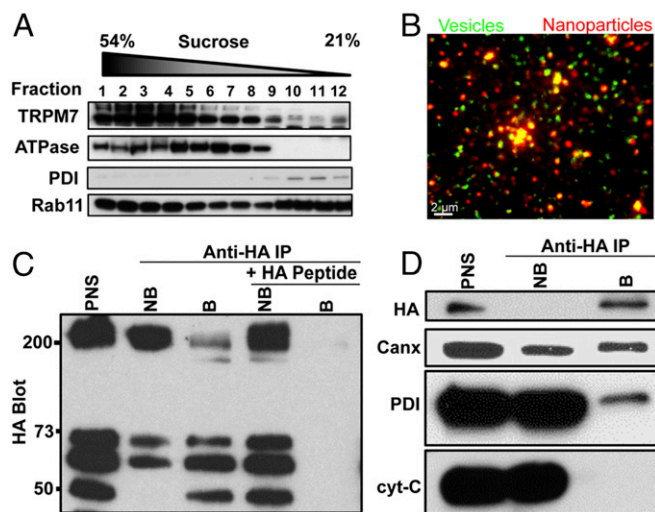


Fig. 3. Purification of M7Vs. (A) Gradient centrifugation of endogenous M7Vs. PNS from SV40MES-13 cells was first separated on a sucrose gradient and then Western blotted for TRPM7, plasma membrane (Na^+/K^+ ATPase), ER (PDI: protein disulfide isomerase), and recycling endosome (Rab11) markers. (B) Postnuclear supernatants of HEK293 cells stably expressing TRPM7-HA (with GCaMP6s in the S1/2 loop) were isolated using mouse anti-HA-conjugated magnetic nanoparticles. Vesicles were visualized by incubation with Ca^{2+} , and nanoparticles were detected with Alexa Fluor 546-conjugated anti-mouse secondary antibodies. (C) Anti-HA Western blot: HA-peptide blocks nanoparticle binding to vesicles. (D) Western blot of isolated vesicles: enrichment of vesicles and depletion of ER (Calnexin; Canx or PDI) and mitochondria (cyt-C). B, Bound; NB, Not bound. See also Fig. S3A.

earlier immunostaining observation that the vesicles are distinct from the ER. Thus, TRPM7 localizes to vesicles that selectively sequester Zn^{2+} upon cytosolic Zn^{2+} overload.

M7Vs Are Enriched in Glutathione. To search for clues about M7Vs' function, we identified metabolites in isolated M7Vs by HPLC-MS. Only glutathione (GSH) was substantially enriched in M7Vs affinity-purified from HEK293 or HEK293T cells, compared with total postnuclear membranes (Dataset S2). We verified the GSH enrichment using a GSH luciferase assay in endogenous vesicles tagged with an HA-epitope inserted at the N terminus of endogenous TRPM7 (Methods). After HA-TRPM7 expression in the ES cells was validated with immunoprecipitation and Western blotting (Fig. S6A), vesicles were affinity purified with anti-HA nanoparticles (Fig. S6B) using the optimized method shown in Fig. 3 B and D. Total GSH was enriched sevenfold in M7Vs compared with total postnuclear membranes (Fig. 6A). Given the central role of GSH in cellular redox reactions, we next determined the redox state of M7Vs in situ using the redox sensor roGFP2 (55) targeted to M7Vs. Although $\sim 10\%$ of cytosolic roGFP2 was oxidized (Fig. 6 B and C), close to the $\sim 5\%$ reported previously (56), $\sim 30\%$ of roGFP2 was oxidized in M7Vs (Fig. 6 B and C). This percentage is significantly greater than the percentage of oxidized roGFP in the cytosol or in mitochondria ($\sim 11\%$) (55) but is much lower than the 96–97% observed in the ER lumen (57, 58) or endolysosomes (94–97%) (57).

Reduced GSH Inhibits Zn^{2+} Passage Through TRPM7. The observation of GSH enrichment in M7Vs motivated us to test whether GSH affects ion conductance through TRPM7. We measured plasma membrane TRPM7 because the extracellular medium can be altered readily to model the M7V lumen. First, Zn^{2+} entry was measured using cytosolic eCALWY4 (Fig. 6D). Overexpression of TRPM7 tripled the rate of Zn^{2+} influx from the extracellular medium, whereas a control, nonconducting TRPM7 pore mutant (33) did not enhance Zn^{2+} influx (Fig. 6 E and F). The addition

of 1 mM GSH, but not glutathione disulfide (GSSG), blocked the TRPM7-dependent Zn^{2+} influx (Fig. 6 G and H) in a dose-dependent manner. To rule out the possibility that the GSH block was caused by Zn^{2+} chelation, we assayed Zn^{2+} binding to Calcium Green-1 [$K_d = 10 \mu\text{M}$ (59)]. As shown in Fig. 6I, 1 mM GSH did not alter the binding of background Zn^{2+} ($\sim 5 \mu\text{M}$) or $50 \mu\text{M}$ Zn^{2+} to Calcium Green-1. Zn^{2+} not only permeates TRPM7 (Fig. 6 E–H) but also blocks both inward and outward monovalent TRPM7 currents with an IC_{50} of $\sim 110 \mu\text{M}$ (Fig. S7 A–C). We conclude that GSH likely prevents Zn^{2+} entry into the TRPM7 pore, an inference supported by patch-clamp experiments demonstrating that GSH, but not GSSG, enhances monovalent TRPM7 currents (Fig. S7E) even in the presence of Zn^{2+} (Fig. S7 E and F).

Oxidation Releases Zn^{2+} from M7Vs in a TRPM7-Dependent Manner. GSH's inhibition of TRPM7's Zn^{2+} conductance suggests that intravesicular reduced GSH enables Zn^{2+} retention in vesicles and that changes in the intravesicular redox state, reflected in the degree of GSH oxidation (60), may regulate Zn^{2+} release. To test oxidation-induced Zn^{2+} release from M7Vs, we transfected WT and TRPM7 $^{-/-}$ HEK293T cells with VIP36-eCALWY4, loaded the cells with Zn^{2+} (as in Fig. 5), and monitored the increase in the mCitrine:mCerulean FRET ratio upon H_2O_2 treatment in Zn^{2+} -free extracellular medium. Exposure to $100 \mu\text{M}$ H_2O_2 resulted in a gradual increase of FRET (i.e., a reduction in Zn^{2+}) in the M7V lumen, which reached a plateau in ~ 30 min (Fig. 7A). The

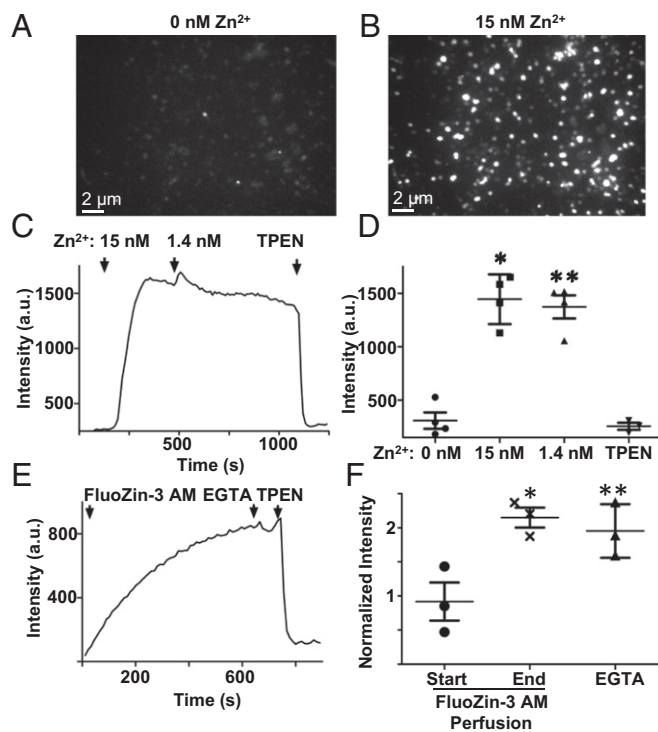


Fig. 4. Zn^{2+} accumulation in purified vesicles. (A and B) M7Vs isolated from SV40MES-13 cells were loaded with FluoZin-3-AM and imaged in medium containing EGTA (A) or 15 nM Zn^{2+} (B). (C and D) Vesicles were perfused first with 15 nM Zn^{2+} and then with 1.4 nM Zn^{2+} or 50 μM TPEN. The mean, SD, and ANOVA statistics from four experiments are shown. $*P < 0.001$ compared with initial fluorescence; $**P < 0.001$ after TPEN addition. (E and F) Zn^{2+} trapping in vesicles is not caused by fluorophore accumulation: Zn^{2+} -loaded vesicles were incubated with FluoZin-3-AM without Zn^{2+} ; then extravesicular dye was washed off, and remaining vesicular fluorescence was reduced by Zn^{2+} chelation by membrane-permeant TPEN but not membrane-impermeant EGTA. Fluorescence intensities in F were normalized to those in TPEN. Results are shown as the mean and SD from three experiments are shown; $*P < 0.05$; ANOVA. See also Fig. S4 A and B.

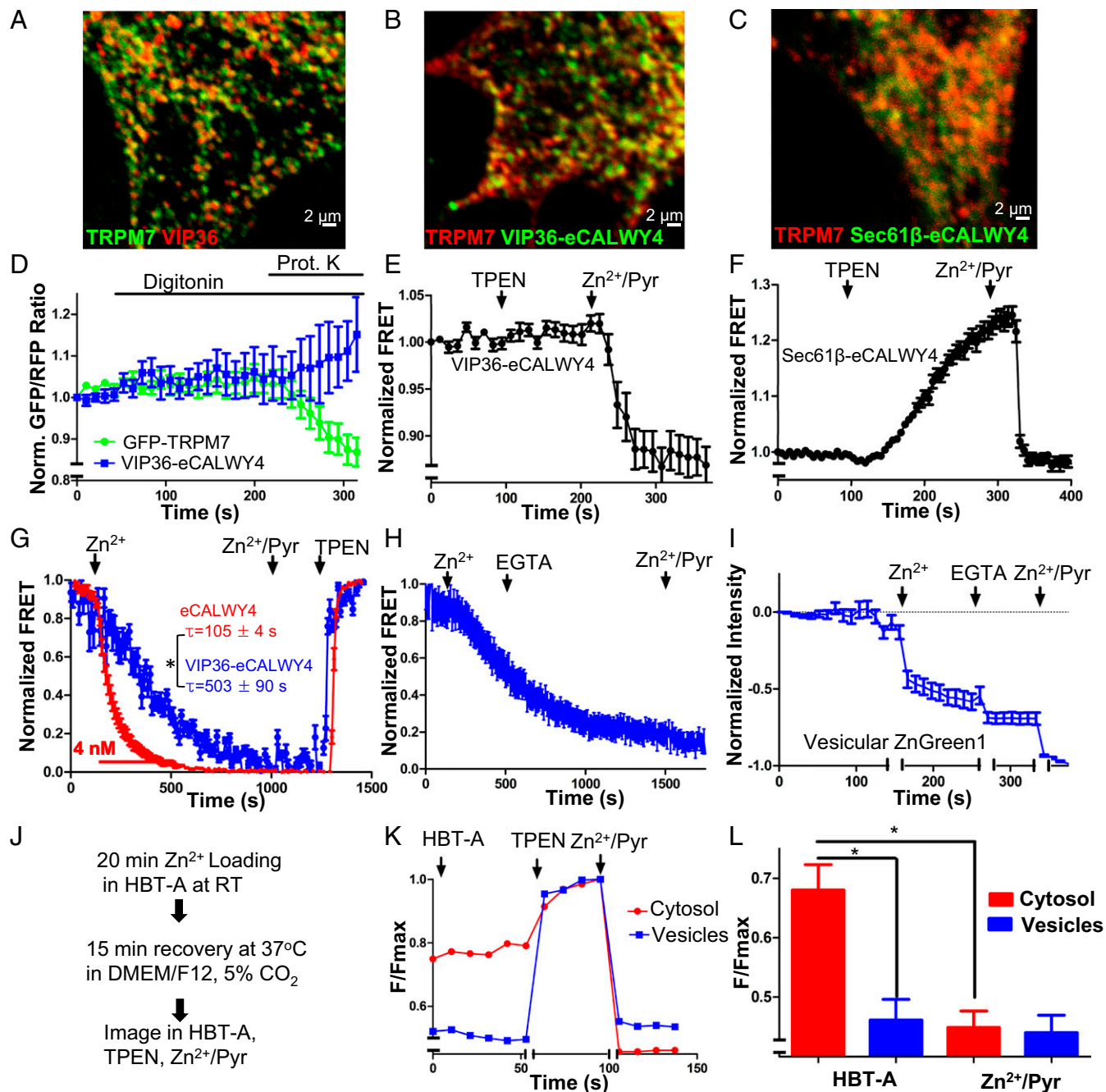


Fig. 5. Zn^{2+} sequestration by M7Vs in intact cells. (A) Colocalization of VIP36-V5 and TRPM7-HA in HEK293 cells. (B) Colocalization of immunostained VIP36-eCALWY4 intravesicular Zn^{2+} sensor and TRPM7-HA in HEK293 cells. (C) Lack of colocalization of ER-targeted eCALWY4 and TRPM7-HA. (D) ER lumen-targeted RCEPIA1er was coexpressed with cytosol-facing GFP (located on the N terminus of TRPM7) or VIP36-eCALWY4. Then the plasma membrane was permeabilized with 20 μM digitonin, and proteinase K was added to digest cytosolic fluorescent proteins. ER lumen-targeted RCEPIA1er was used as a proteinase K-inaccessible control. (E) HEK293 cells expressing VIP36-eCALWY4 were incubated with 50 μM TPEN or 50 μM Zn^{2+} /20 μM pyrithione. Shown are means and SEMs of seven cells in more than four representative time-course experiments. (F) eCALWY4 was targeted into the ER lumen using Sec61 β , and cells were imaged in 50 μM TPEN or 50 μM Zn^{2+} /20 μM pyrithione. Shown are the mean and SEM of seven cells in a representative time-course experiment. (G) HEK293 cells were transfected with either VIP36-eCALWY4 or eCALWY4 cDNA and then were incubated with 500 μM Zn^{2+} , followed by 50 μM Zn^{2+} /20 μM pyrithione and TPEN. Shown are time constants of Zn^{2+} entry and 95% CIs of 10–12 cells representative of multiple similar experiments; * $P < 0.0001$ after an extra sum of squares F -test comparison of the two curves. (H) Vesicular Zn^{2+} loading was initiated with 500 μM extracellular Zn^{2+} , which then was replaced with 250 μM EGTA to chelate Zn^{2+} . The mean and SEM of data from 19 cells from three experiments are plotted. (I) Cells expressing TRPM7 (ZnGreen1 inserted between the S1 and S2 domains of TRPM7) were perfused with Zn^{2+} and EGTA as in *H*. Plots show means and SEMs of cells from one experiment representative of more than three; axis breaks are 5 min. (J) The method for loading and releasing Zn^{2+} from M7Vs with luminal ZnGreen1. (K and L) After cytosolic and M7V-luminal ZnGreen1 were saturated with Zn^{2+} and cells were allowed to extrude cytosolic Zn^{2+} as described in *J*, residual cytosolic and vesicular Zn^{2+} were imaged in 50 μM HBT-A or 50 μM TPEN Zn^{2+} /20 μM pyrithione. * $P < 0.05$, ANOVA after Tukey's multiple comparison test of 24–36 cells from three experiments. See also [Figs. S2–S5](#) and [Dataset S1](#).

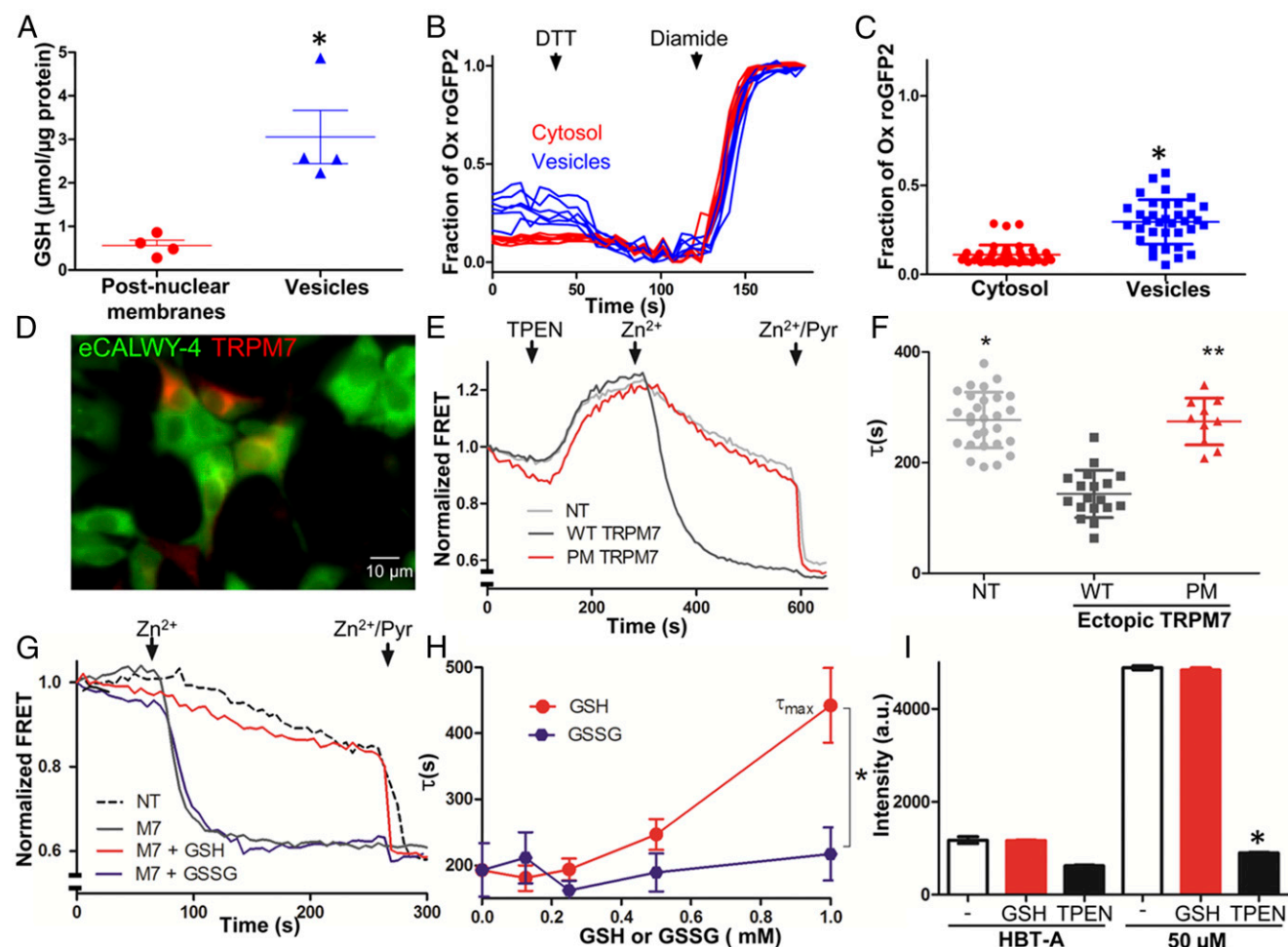


Fig. 6. Regulation of TRPM7-mediated Zn^{2+} entry by the glutathione redox state. (A) Luciferase assay of GSH in postnuclear membranes and M7Vs purified from ES cells expressing HA-tagged endogenous TRPM7. The mean and SD of four replicates are plotted and compared by Student's *t* test; $*P < 0.01$. (B and C) Cytosolic or intravesicular roGFP2 was maximally reduced with 10 mM DTT and maximally oxidized with 1 mM diamide in HBT-A. $*P < 0.001$ by Student's *t* test, $n = 35$ –42 cells. (D) HEK293 cells expressing eCALWY4 without (green only) or with mCherry-TRPM7 (green and red). (E) Time-course of Zn^{2+} entry into nontransfected HEK293 cells (NT, gray line), HEK293 cells overexpressing WT mCherry-TRPM7 (WT, black line), or loss-of-function pore-mutant mCherry-TRPM7 (PM, red line). After baseline imaging in HBT-A, cells were perfused with the Zn^{2+} chelator TPEN, followed by 50 μ M Zn^{2+} and 50 μ M $Zn^{2+}/20$ μ M pyrithione (Zn^{2+}/Pyr) at the time points indicated by black arrows. (F) Time constants of Zn^{2+} entry into nontransfected and TRPM7-overexpressing HEK293 cells. Means and SD are plotted along with results of ANOVA with Kruskal–Wallis post test; asterisks indicate $P < 0.05$ compared with WT TRPM7-transfected cells. (G) Comparison of the effects of GSH (red line) and GSSG (purple line) on Zn^{2+} entry into HEK293 cells expressing eCALWY4 without (dashed line) or with (solid lines) mCherry-TRPM7. (H) Dose-dependence of GSH/GSSG effects on Zn^{2+} entry. τ_{max} is the maximum time constant for Zn^{2+} entry (no inhibition); $n = 3$ –10 cells; error bars indicate SEM. $*P < 0.001$. (I) Responses of Calcium Green-1 (low-affinity Zn^{2+} indicator), to Zn^{2+} in 100 μ M TPEN or 1 mM GSH. The means and SEMs of three to six replicates are plotted; $*P < 0.05$ by ANOVA followed by a Kruskal–Wallis post test; a.u., arbitrary units. See Figs. S6 and S7 and Dataset S2.

FRET increase was substantially reduced in TRPM7^{-/-} cells compared with WT cells (Fig. 7 B and C), indicating that TRPM7 mediates oxidation-induced Zn^{2+} release from vesicles.

The initial reduction of the FRET ratio of the Zn^{2+} -saturated sensor by H₂O₂ (Fig. 7 A and B) raised the possibility that eCALWY was modified by oxidation. We therefore used FluoZin-3 in place of genetically encoded protein sensors to monitor cytosolic Zn^{2+} in subsequent experiments, because previous studies have shown that FluoZin-3 responses to Zn^{2+} are not altered by H₂O₂ or ROS (61, 62). H₂O₂ increased Zn^{2+} (FluoZin-3 fluorescence) in Zn^{2+} -loaded WT cells but not in TRPM7^{-/-} cells (Fig. 7 D–F). Because the extracellular solution did not contain significant Zn^{2+} (<0.2 nM), we conclude that the source of the TRPM7-dependent, H₂O₂-induced increase in cytosolic Zn^{2+} was the M7V.

Finally, we tested whether endogenous ROS generation triggered by oxygen–glucose deprivation (OGD) (63, 64) elicits

Zn^{2+} release into the cytosol through TRPM7. OGD with glucose-free sodium dithionite resulted in a wave of Zn^{2+} release, as recently reported (62), in WT but not in TRPM7^{-/-} HEK293T cells (Fig. 7 G–I). The OGD-induced Zn^{2+} release was rescued by ectopic TRPM7 expression in TRPM7^{-/-} cells (Fig. 7J). Again, because the extracellular solution did not contain significant Zn^{2+} , we conclude that M7Vs were the source of TRPM7-dependent, OGD-induced increase in cytosolic Zn^{2+} . In conclusion, TRPM7 forms functional intracellular channels that mediate Zn^{2+} release from the lumen of a previously unrecognized population of vesicles during oxidative stress.

Discussion

Our prior observations of intracellular TRPM7 on 50- to 250-nm vesicles led us to investigate the existence of an additional and perhaps more important function of TRPM7 as an intracellular channel. Here we show that most TRPM7 forms intracellular

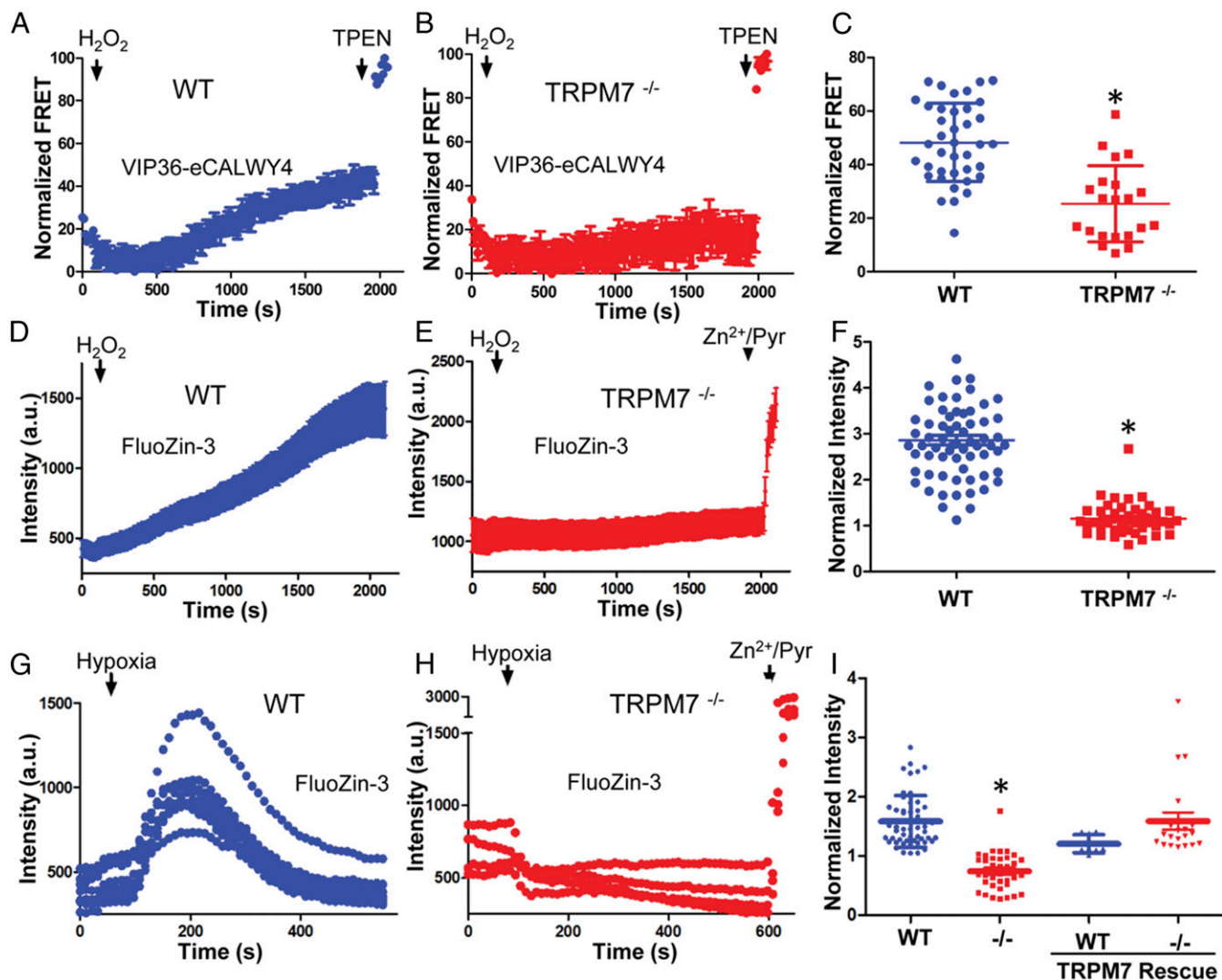


Fig. 7. TRPM7 is required for ROS-induced Zn²⁺ release from intracellular stores. (A–C) Zn²⁺ release from M7Vs was monitored in WT (A and C) or TRPM7^{-/-} (B and C) HEK293T cells expressing the VIP36-eCALWY4 intravesicular Zn²⁺ sensor. Cells first were incubated with 500 μ M Zn²⁺ and then were perfused with 100 μ M H₂O₂ in Zn²⁺-free HBT-A containing 250 μ M EGTA and 4 mM MgCl₂. WT and TRPM7^{-/-} cells were compared by Student's *t* test; **P* < 0.0001, *n* = 21–39 cells. (D–F) FluoZin-3-loaded WT (D and F) or TRPM7^{-/-} (E and F) HEK293T cells were similarly loaded with Zn²⁺ and then were treated with H₂O₂ in Zn²⁺-free extracellular medium. The means and SEMs of 44–67 cells are plotted; **P* < 0.0001 compared with WT, Student's *t* test. (G–I) Experiments were performed as in A–F, but 10 mM sodium dithionite, instead of H₂O₂, was applied to induce Zn²⁺ release from intracellular stores, and glucose was omitted from HBT-A. WT mCherry-TRPM7 was overexpressed to rescue the Zn²⁺ release in TRPM7^{-/-} cells. The means and SEMs of 8–30 cells are plotted; **P* < 0.0001 compared with WT, Student's *t* test. a.u., arbitrary units.

Zn²⁺-release channels in a previously unrecognized type of Zn²⁺-storage vesicle in multiple cell types. Oxidizing conditions activate intracellular Zn²⁺ release via TRPM7, likely by converting GSH in M7Vs to GSSG. We anticipate these findings will provide insights into the cellular function of TRPM7.

Several transient receptor potential (TRP) channels function in various intracellular compartments. For example, TRPML1 and TRPM2 release lysosomal Ca²⁺ and Zn²⁺, whereas TRPM8 may release Ca²⁺ from the ER in some cell types (65, 66). The *Drosophila* TRPM channel, proposed to release Zn²⁺ from intracellular stores during larval development, exhibits TRPM7-like currents (67). We now include TRPM7 in the class of functional intracellular TRP channels. However, the intracellular function of TRPM7 is unique in two ways. First, TRPM7 functions in vesicles that are distinct from known compartments. Second, unlike ER and lysosomes that store both Ca²⁺ and Zn²⁺, M7Vs store only Zn²⁺.

Under resting conditions, M7Vs do not contain free Zn²⁺, unlike intracellular Zn²⁺ stores such as mitochondria, ER, lysosomes, synaptic vesicles, and zinosomes (42). Although GSH is enriched in M7Vs and does not chelate micromolar [Zn²⁺] in physiological solutions, it may still bind Zn²⁺ under some conditions that may exist in M7Vs (68). The complex dynamics of cellular redox status and M7V GSH content, cytoplasmic free Mg²⁺, and ATP (as well as other phosphonucleotides) will require careful examination in the future.

M7Vs are uniformly distributed in the cell and thus are an ideal ion storage system. We hypothesize that M7Vs sequester Zn²⁺ to protect other organelles, but because Zn²⁺ binds many proteins, DNA, and RNA, the vesicles also could release Zn²⁺ to alter many cellular processes. We are exploring the possibility that Zn²⁺ released from M7Vs regulates TRPM7 kinase cleavage, activity, or trafficking. Furthermore, the proteomics data in this study suggest that dozens of proteins are localized, at least partially, in M7Vs. In this study, we focused on iden-

tifying probes for the lumens of M7Vs, but verification of the full complement of M7V proteins will elucidate their biogenesis and function. The presence of vesicle trafficking proteins (e.g., vesicle-associated membrane protein A, VAPA) and fusion proteins (e.g., vesicle-associated membrane protein 1, VAMP1, and extended syntaptotagmin-1, ESYT1) in the M7V proteome is consistent with the previously reported M7V exocytosis during shear stress and cholinergic synaptic transmission (33, 34). Enrichment of ferritin light chain in vesicles isolated from SV40MES cells also suggests the possibility of iron storage by M7Vs. Our M7V proteome did not contain transporters for divalent cations (e.g., ZnTs, ZiPs, or other divalent metal transporters) or GSH, likely because these proteins are not highly expressed, but targeted proteomic analysis may reveal their identities.

Total Zn^{2+} increases by 50% during meiotic maturation of oocytes; about half of this increase is released by vesicular exocytosis within minutes of fertilization (69), and the rest persists through preimplantation (70). Because TRPM7 is required for preimplantation development (71), it will be important to determine if the Zn^{2+} -containing vesicles in oocytes and early embryos are M7Vs and how changes in GSH/redox during early development (31, 72, 73) may regulate Zn^{2+} uptake and release from M7Vs. In postnatal animals, extracellular free $[Zn^{2+}]$ can rise to several hundred micromolar during ischemia or seizures (16, 17, 74), comparable to the levels required to fill M7Vs in these studies. Zn^{2+} also may be redistributed from other intracellular sites into M7Vs. These include mitochondria and NADPH oxidase at the plasma membrane, major sites of ROS that liberate Zn^{2+} from the mitochondrial matrix and from metallothioneins (16, 17, 74). Thus, M7Vs may comprise a sink or reservoir buffering cytosolic Zn^{2+} .

Experimental Procedures

Detailed methods are available in *SI Experimental Procedures*.

Immunofluorescence Microscopy. Cells were fixed in 4% paraformaldehyde and permeabilized in 0.1% Triton-X 100 at room temperature. Nonspecific binding was blocked with 10% goat serum in PBS, and cells were incubated in primary antibodies for 2 h at room temperature or overnight at 4 °C, followed by detection with fluorophore-conjugated secondary antibodies. Cells then were imaged by confocal or STED microscopy.

TEM. Transfected cells were fixed in 1% paraformaldehyde in PBS, permeabilized, blocked, and incubated with anti-GFP antibody overnight. After rinsing, cells were labeled with protein-A-conjugated 10-nm colloidal gold (Aurion) or 1.4-nm FluoroNanogold-conjugated secondary antibodies (Nanoprobes); the latter were silver enhanced. Cells then were postfixed in 1% glutaraldehyde, and 10-nm-thin slices were imaged by TEM.

Tagging of Endogenous TRPM7. TRPM7 was tagged as described in ref. 75. Briefly, ES cells with gene-trapped TRPM7 were purchased from the European Mammalian Mutant Cell Repository (EuMMCR) and verified by genotyping the regions flanking exon 1 of TRPM7. The cells then were electroporated with plasmids encoding GFP or HA-SNAP tags and flippase (FLP) recombinase. ES cell clones with tagged TRPM7 were selected with hygromycin.

- Nadler MJ, et al. (2001) LTRPC7 is a Mg₂-ATP-regulated divalent cation channel required for cell viability. *Nature* 411:590–595.
- Runnels LW, Yue L, Clapham DE (2001) TRP-PLIK, a bifunctional protein with kinase and ion channel activities. *Science* 291:1043–1047.
- Jin J, et al. (2008) Deletion of *Trpm7* disrupts embryonic development and thymopoiesis without altering Mg²⁺ homeostasis. *Science* 322:756–760.
- Jin J, et al. (2012) The channel kinase, TRPM7, is required for early embryonic development. *Proc Natl Acad Sci USA* 109:E225–E233.
- Aarts M, et al. (2003) A key role for TRPM7 channels in anoxic neuronal death. *Cell* 115:863–877.
- Bae CY, Sun HS (2013) Current understanding of TRPM7 pharmacology and drug development for stroke. *Acta Pharmacol Sin* 34:10–16.
- Monteilh-Zoller MK, et al. (2003) TRPM7 provides an ion channel mechanism for cellular entry of trace metal ions. *J Gen Physiol* 121:49–60.
- Krapivinsky G, Krapivinsky L, Manasian Y, Clapham DE (2014) The TRPM7 chanzyme is cleaved to release a chromatin-modifying kinase. *Cell* 157:1061–1072.

Affinity Purification of TRPM7-Containing Vesicles. SV40MES-13 cells stably expressing GFP-TRPM7-HA or HEK293 cells stably expressing GCaMP6s-TRPM7-HRV3C-HA were homogenized and centrifuged to obtain PNS. The PNS was incubated with mouse anti-HA-conjugated magnetic nanoparticles (Miltenyi Biotec) and were loaded onto LS columns (Miltenyi Biotec). After rinsing, immobilized vesicles were eluted in PBS. For proteomic analysis eluted vesicles were isolated again with anti-FLAG-conjugated magnetic nanoparticles.

Metabolomics. M7Vs were isolated from HEK293 or HEK293T cells stably expressing GCaMP6s-TRPM7-HA using anti-HA nanoparticles as described above. They then were vortexed in 0.9% NaCl and centrifuged; supernatants were used for LC-MS sample extractions.

Imaging of Zn^{2+} Flux with Genetically Encoded Zn^{2+} Sensors. HEK293 cells transfected with eCALWY4 or with eCALWY4 and mCherry-TRPM7 were imaged as described in ref. 47. To study Zn^{2+} flux in intracellular compartments, HEK293 cells expressing intravesicular Zn^{2+} sensors were imaged in HBT-A medium (20 mM Hepes, 120 mM NaCl, 0.8 mM MgCl₂, 1.8 mM CaCl₂, 10 mM glucose, pH 7.5) with or without extracellular Zn^{2+} .

Live Imaging of Vesicular Redox Environment. A ratiometric redox sensor, roGFP2, was targeted to the lumen of M7Vs by insertion between the S1 and S2 domains of TRPM7. After baseline image acquisition, the sensor was maximally reduced with 10 mM DTT (Bio-Rad) and then maximally oxidized in 1 mM diamide (Sigma).

Zn^{2+} Release from Intracellular Stores. Untransfected (FluoZin-3-loaded) or VIP36-eCALWY4-transfected WT and TRPM7^{-/-} HEK293T cells were incubated with 500 μ M Zn^{2+} in Mg²⁺- and Ca²⁺-free solution for 10–20 min. The cells then were perfused with 10 mM sodium dithionite (in glucose-free) or 100 μ M H₂O₂ (in normal) HBT-A medium containing 0.25 mM EGTA to chelate Zn^{2+} and 4 mM Mg²⁺ to block plasma membrane-localized TRPM7.

TRPM7 Deletion in HEK293T Cells. A variant of the CRISPR/Cas9 method (76) was used to insert puromycin- and blasticidin-coding sequences into the second exon of *Trpm7*. The donor DNA contained the predicted coding sequence of *Trpm7*'s first 12 amino acids followed by an antibiotic resistance cassette, multiple stop codons, and SV40-polyA. Oligonucleotides encoding the genomic RNA (gRNA) sequence were annealed and cloned into BPK1520 (77). Donor DNA containing puromycin-SV40pA and blasticidin-SV40pA cassettes were amplified from pPur (Clontech) and pcDNA6-V5-His (Invitrogen), respectively, with primers flanked with a target site on exon 2 of TRPM7 and were ligated into a pJET1.2 cloning vector (Thermo Fisher). HEK293T cells then were transfected with the BPK1520 construct and the puromycin resistance cassette donor template using Lipofectamine LTX (Thermo Fisher). Puromycin-resistant cells were cloned and genotyped, and knockout of *Trpm7* was verified by immunoprecipitation, Western blotting, and electrophysiology.

Statistical Analyses. Data were plotted and analyzed in Prism 5 (GraphPad) by Student's *t* tests, ANOVA with Tukey's post hoc tests, or extra sum of squares F-tests (for nonlinear regressions).

ACKNOWLEDGMENTS. We thank Maria Ericsson for EM, Clary Clish for metabolomics, Eric Spooner for proteomics studies, Bayush Dinegde for DNA purification, Svetlana Gapon for cell culture, and Luba Krapivinsky for TRPM7 antibody purification. This work was supported in part by NIH Institutional Research Training (T32) Grants 5T32HL007572-31 (to S.A.A.) and K99HL124070 (to D.C.) at Boston Children's Hospital.

- Inoue K, Branigan D, Xiong ZG (2010) Zinc-induced neurotoxicity mediated by transient receptor potential melastatin 7 channels. *J Biol Chem* 285:7430–7439.
- Castillo B, Pörzgen P, Penner R, Horgen FD, Fleig A (2010) Development and optimization of a high-throughput bioassay for TRPM7 ion channel inhibitors. *J Biomol Screen* 15:498–507.
- Dorovkov MV, Ryzanov AG (2004) Phosphorylation of annexin I by TRPM7 channel-kinase. *J Biol Chem* 279:50643–50646.
- Clark K, et al. (2006) TRPM7, a novel regulator of actomyosin contractility and cell adhesion. *EMBO J* 25:290–301.
- Su LT, et al. (2006) TRPM7 regulates cell adhesion by controlling the calcium-dependent protease calpain. *J Biol Chem* 281:11260–11270.
- Desai BN, et al. (2012) Cleavage of TRPM7 releases the kinase domain from the ion channel and regulates its participation in Fas-induced apoptosis. *Dev Cell* 22:1149–1162.
- Vallee BL, Falchuk KH (1993) The biochemical basis of zinc physiology. *Physiol Rev* 73: 79–118.

16. Choi DW, Koh JY (1998) Zinc and brain injury. *Annu Rev Neurosci* 21:347–375.
17. Frederickson CJ, Koh J-Y, Bush AI (2005) The neurobiology of zinc in health and disease. *Nat Rev Neurosci* 6:449–462.
18. McCord MC, Aizenman E (2014) The role of intracellular zinc release in aging, oxidative stress, and Alzheimer's disease. *Front Aging Neurosci* 6:77.
19. Schmitz C, et al. (2003) Regulation of vertebrate cellular Mg²⁺ homeostasis by TRPM7. *Cell* 114:191–200.
20. Quamme GA (2010) Molecular identification of ancient and modern mammalian magnesium transporters. *Am J Physiol Cell Physiol* 298:C407–C429.
21. Runnels LW, Yue L, Clapham DE (2002) The TRPM7 channel is inactivated by PIP(2) hydrolysis. *Nat Cell Biol* 4:329–336.
22. Romani AM (2011) Cellular magnesium homeostasis. *Arch Biochem Biophys* 512:1–23.
23. Kambe T, Tsuji T, Hashimoto A, Itsumura N (2015) The physiological, biochemical, and molecular roles of zinc transporters in zinc homeostasis and metabolism. *Physiol Rev* 95:749–784.
24. Baldoli E, Castiglioni S, Maier JA (2013) Regulation and function of TRPM7 in human endothelial cells: TRPM7 as a potential novel regulator of endothelial function. *PLoS One* 8:e59891.
25. Wuensch T, et al. (2010) High glucose-induced oxidative stress increases transient receptor potential channel expression in human monocytes. *Diabetes* 59:844–849.
26. Sun H, et al. (2013) Role of TRPM7 channels in hyperglycemia-mediated injury of vascular endothelial cells. *PLoS One* 8:e79540.
27. Demir T, et al. (2014) Evaluation of TRPM (transient receptor potential melastatin) genes expressions in myocardial ischemia and reperfusion. *Mol Biol Rep* 41:2845–2849.
28. Chen W, et al. (2015) TRPM7 inhibitor carvacrol protects brain from neonatal hypoxic-ischemic injury. *Mol Brain* 8:11.
29. Bae CY, Sun HS (2011) TRPM7 in cerebral ischemia and potential target for drug development in stroke. *Acta Pharmacol Sin* 32:725–733.
30. Bigarella CL, Liang R, Ghaffari S (2014) Stem cells and the impact of ROS signaling. *Development* 141:4206–4218.
31. Dunwoodie SL (2009) The role of hypoxia in development of the mammalian embryo. *Dev Cell* 17:755–773.
32. Mori Y, et al. (2016) Redox-sensitive transient receptor potential channels in oxygen sensing and adaptation. *Pflugers Arch* 468:85–97.
33. Krapivinsky G, Mochida S, Krapivinsky L, Cibulsky SM, Clapham DE (2006) The TRPM7 ion channel functions in cholinergic synaptic vesicles and affects transmitter release. *Neuron* 52:485–496.
34. Oancea E, Wolfe JT, Clapham DE (2006) Functional TRPM7 channels accumulate at the plasma membrane in response to fluid flow. *Circ Res* 98:245–253.
35. Brauchi S, Krapivinsky G, Krapivinsky L, Clapham DE (2008) TRPM7 facilitates cholinergic vesicle fusion with the plasma membrane. *Proc Natl Acad Sci USA* 105:8304–8308.
36. Lange I, et al. (2009) TRPM2 functions as a lysosomal Ca²⁺-release channel in beta cells. *Sci Signal* 2:ra23.
37. Manna PT, et al. (2015) TRPM2-mediated intracellular Zn²⁺ release triggers pancreatic β -cell death. *Biochem J* 466:537–546.
38. Hoock TC, Newcomb PM, Herman IM (1991) Beta actin and its mRNA are localized at the plasma membrane and the regions of moving cytoplasm during the cellular response to injury. *J Cell Biol* 112:653–664.
39. Miesenböck G, De Angelis DA, Rothman JE (1998) Visualizing secretion and synaptic transmission with pH-sensitive green fluorescent proteins. *Nature* 394:192–195.
40. Presley JF, et al. (1997) ER-to-Golgi transport visualized in living cells. *Nature* 389:81–85.
41. Noack J, Bernasconi R, Molinari M (2014) How viruses hijack the ERAD tuning machinery. *J Virol* 88:10272–10275.
42. Palmiter RD, Cole TB, Findley SD (1996) ZnT-2, a mammalian protein that confers resistance to zinc by facilitating vesicular sequestration. *EMBO J* 15:1784–1791.
43. Füllekrug J, Scheiffele P, Simons K (1999) VIP36 localisation to the early secretory pathway. *J Cell Sci* 112:2813–2821.
44. Hara-Kuge S, et al. (2002) Involvement of VIP36 in intracellular transport and secretion of glycoproteins in polarized Madin-Darby canine kidney (MDCK) cells. *J Biol Chem* 277:16332–16339.
45. Shimada O, et al. (2003) Localization of VIP36 in the post-Golgi secretory pathway also of rat parotid acinar cells. *J Histochem Cytochem* 51:1057–1063.
46. Shirakabe K, Hattori S, Seiki M, Koyasu S, Okada Y (2011) VIP36 protein is a target of ectodomain shedding and regulates phagocytosis in macrophage Raw 264.7 cells. *J Biol Chem* 286:43154–43163.
47. Vinkenborg JL, et al. (2009) Genetically encoded FRET sensors to monitor intracellular Zn²⁺ homeostasis. *Nat Methods* 6:737–740.
48. Miranda JG, et al. (2012) New alternately colored FRET sensors for simultaneous monitoring of Zn²⁺ in multiple cellular locations. *PLoS One* 7:e49371.
49. Qin Y, Dittmer PJ, Park JG, Jansen KB, Palmer AE (2011) Measuring steady-state and dynamic endoplasmic reticulum and Golgi Zn²⁺ with genetically encoded sensors. *Proc Natl Acad Sci USA* 108:7351–7356.
50. Chabosseau P, et al. (2014) Mitochondrial and ER-targeted eCALWY probes reveal high levels of free Zn²⁺. *ACS Chem Biol* 9:2111–2120.
51. Chen Z, Ai HW (2016) Single fluorescent protein-based indicators for zinc ion (Zn²⁺). *Anal Chem* 88:9029–9036.
52. Chen TW, et al. (2013) Ultrasensitive fluorescent proteins for imaging neuronal activity. *Nature* 499:295–300.
53. Suzuki J, et al. (2014) Imaging intraorganellar Ca²⁺ at subcellular resolution using CEPIA. *Nat Commun* 5:4153.
54. Zhao Y, et al. (2011) An expanded palette of genetically encoded Ca²⁺ indicators. *Science* 333:1888–1891.
55. Hanson GT, et al. (2004) Investigating mitochondrial redox potential with redox-sensitive green fluorescent protein indicators. *J Biol Chem* 279:13044–13053.
56. Dooley CT, et al. (2004) Imaging dynamic redox changes in mammalian cells with green fluorescent protein indicators. *J Biol Chem* 279:22284–22293.
57. Austin CD, et al. (2005) Oxidizing potential of endosomes and lysosomes limits intracellular cleavage of disulfide-based antibody-drug conjugates. *Proc Natl Acad Sci USA* 102:17987–17992.
58. Birk J, et al. (2013) Endoplasmic reticulum: Reduced and oxidized glutathione revisited. *J Cell Sci* 126:1604–1617.
59. Martin JL, Stork CJ, Li YV (2006) Determining zinc with commonly used calcium and zinc fluorescent indicators, a question on calcium signals. *Cell Calcium* 40:393–402.
60. Wu G, Fang YZ, Yang S, Lupton JR, Turner ND (2004) Glutathione metabolism and its implications for health. *J Nutr* 134:489–492.
61. Huang YZ, McNamara JO (2012) Neuroprotective effects of reactive oxygen species mediated by BDNF-independent activation of TrkB. *J Neurosci* 32:15521–15532.
62. Slepchenko KG, Lu Q, Li YV (2016) Zinc wave during the treatment of hypoxia is required for initial reactive oxygen species activation in mitochondria. *Int J Physiol Pathophysiol Pharmacol* 8:44–51.
63. Sena LA, Chandel NS (2012) Physiological roles of mitochondrial reactive oxygen species. *Mol Cell* 48:158–167.
64. Sabharwal SS, Schumacker PT (2014) Mitochondrial ROS in cancer: Initiators, amplifiers or an Achilles' heel? *Nat Rev Cancer* 14:709–721.
65. Dong XP, Wang X, Xu H (2010) TRP channels of intracellular membranes. *J Neurochem* 113:313–328.
66. Gees M, Colsoul B, Nilius B (2010) The role of transient receptor potential cation channels in Ca²⁺ signaling. *Cold Spring Harb Perspect Biol* 2:a003962.
67. Georgiev P, et al. (2010) TRPM channels mediate zinc homeostasis and cellular growth during Drosophila larval development. *Cell Metab* 12:386–397.
68. Krezel A, Bal W (2004) Studies of zinc(II) and nickel(II) complexes of GSH, GSSG and their analogs shed more light on their biological relevance. *Bioinorg Chem Appl* 2:293–305.
69. Kim AM, Vogt S, O'Halloran TV, Woodruff TK (2010) Zinc availability regulates exit from meiosis in maturing mammalian oocytes. *Nat Chem Biol* 6:674–681.
70. Kong BY, et al. (2015) The inorganic anatomy of the mammalian preimplantation embryo and the requirement of zinc during the first mitotic divisions. *Dev Dyn* 244:935–947.
71. Carvacho I, et al. (2016) TRPM7-like channels are functionally expressed in oocytes and modulate post-fertilization embryo development in mouse. *Sci Rep* 6:34236.
72. Gardiner CS, Reed DJ (1994) Status of glutathione during oxidant-induced oxidative stress in the preimplantation mouse embryo. *Biol Reprod* 51:1307–1314.
73. Nasr-Esfahani MH, Johnson MH (1992) Quantitative analysis of cellular glutathione in early preimplantation mouse embryos developing in vivo and in vitro. *Hum Reprod* 7:1281–1290.
74. Jeong J, et al. (2012) Promotion of vesicular zinc efflux by ZIP13 and its implications for spondylocheiro dysplastic Ehlers-Danlos syndrome. *Proc Natl Acad Sci USA* 109:E3530–E3538.
75. Schnütgen F, et al. (2011) Resources for proteomics in mouse embryonic stem cells. *Nat Methods* 8:103–104.
76. Nakade S, et al. (2014) Microhomology-mediated end-joining-dependent integration of donor DNA in cells and animals using TALENs and CRISPR/Cas9. *Nat Commun* 5:5560.
77. Kleinstiver BP, et al. (2015) Engineered CRISPR-Cas9 nucleases with altered PAM specificities. *Nature* 523:481–485.
78. Dittmer PJ, Miranda JG, Gorski JA, Palmer AE (2009) Genetically encoded sensors to elucidate spatial distribution of cellular zinc. *J Biol Chem* 284:16289–16297.
79. White C, Nixon A, Bradbury NA (2015) Determining membrane protein topology using fluorescence protease protection (FPP). *J Vis Exp* 98:e52509.
80. Mi H, Muruganujan A, Casagrande JT, Thomas PD (2013) Large-scale gene function analysis with the PANTHER classification system. *Nat Protoc* 8:1551–1566.